1

NARROW LINE REGION PROPERTIES

1.1 INTRODUCTION

AGN appear to to be very efficient at driving outflows, and X-ray and UV spectroscopy reveal high velocity outflows to be nearly ubiquituous on sub-parsec scales in high accretion rate quasars. In recent years, a huge amount of resources have been devoted to searching for observational evidence of galaxy-wide, AGN-driven ouflows, which could provide the feedback mechanism nessecary to quench star formation in massive galaxies. This has resulted in recent detections of winds in AGN-host galaxies using tracers of atomic, molecular, and inoised gas (e.g. Nesvadba et al., 2006; Arav et al., 2008; Nesvadba et al., 2008; Moe et al., 2009; Dunn et al., 2010; Alexander et al., 2010; Harrison et al., 2012; Harrison et al., 2014; Nesvadba et al., 2010; Rupke and Veilleux, 2013; Veilleux et al., 2013; Nardini et al., 2015; Feruglio et al., 2010; Alatalo et al., 2011; Cimatti et al., 2013; Cicone et al., 2014).

One particularly successful technique has been observations of forbiden emission lines, which trace warm (T$\sim 10^4$K) ionised gas in the narrow line region (NLR). Because of its high equivalent width, [O III]λ5008 is most studied of the narrow quasar emission lines. In general, the [O III] emission appears to consist of two components: a narrow, 'core' component, with a velocity close to the systemic redshift of the host galaxy, and a broader 'wing' component, which is normally blueshifted. The general consensus is that the core component traces the gravitational potential of the host galaxy, whereas the wing is tracing outflowing gas.

Observations of broad velocity-widths and asymetries in narrow emission lines stretch back several decades (e.g. Weedman, 1970; Stockton, 1976; Heckman et al., 1981; Veron, 1981; Feldman et al., 1982; Heckman, Miley, and Green, 1984; Vrtilek, 1985; Whittle, 1985; Boroson and Green, 1992). However, the small sample sizes make it difficult to know how representative these observations are. More recently, the advent of large optical spectroscopic surveys (e.g. SDSS) have facilitated studies of the NLR in tens of thousands of AGN (e.g. Boroson, 2005; Greene and Ho, 2005; Zhang et al., 2011; Mullaney et al., 2013; Zakamska and Greene, 2014; Shen and Ho, 2014). This has provided constraints on the prevalence of ionised outflows and, by measuring outflow properties as a function of AGN properties, on the drivers of these outflows. At the same time, there is strong evidence from spatially resolved spectroscopic observations of kine-

matically disturbed gas extended over galaxy scales (e.g. Greene et al., 2009; Greene et al., 2011; Hainline et al., 2013; Harrison et al., 2012; Harrison et al., 2014).

However, these studies do not cover the redshift range when star formation and black hole accretion peaked, and consequently when feedback is predicted to be strongest. At these redshifts the bright optical emission lines are redshifted to near-infrared wavelengths, where observations are much more challenging compared to optical wavelengths. As a consequence, studies at high redshifts have typically relied on relatively small numbers of objects, which might not be representative of the properties of the population (e.g. Netzer et al., 2004; Sulentic et al., 2004; Shen, 2016). Other recent studies have looked at the [O III] emission properties of rare sub-samples - e.g. heavily obscured quasars (Zakamska et al., 2016) and the most luminous quasars (Bischetti et al., 2016). These studies often report exceptionally large [O III] widths, with FWHM $> 1000 \mathrm{km\,s^{-1}}$(e.g. Netzer et al., 2004; Nesvadba et al., 2008; Kim et al., 2013; Brusa et al., 2015; Carniani et al., 2015; Perna et al., 2015; Bischetti et al., 2016). This could suggets that AGN efficiency in driving galaxy-wide outflows increases with AGN luminosity (e.g. Hopkins et al. 2016). In addition, [O III] is often very weak, or is missing entirely (e.g. Netzer et al., 2004).

In this chapter we analyse the [O III] properties of a sample of 345 high-luminosity, redshift $1.5 < z < 4$ quasars. The large sample size will help to put these observations in context of the AGN population as a whole. We will analyse the [O III] emission properties as a function of key properties of the quasar, e.g. BH mass, luminosity, and accretion rate.

1.2 QUASAR SAMPLE

We have assembled a catalogue of 345 high-luminosity, redshift $1.5 < z < 4$ quasars, with high-quality near-infrared spectra covering the broad Balmer Hβ line and the strong, narrow [O III] doublet. This is the largest study of the narrow line region properties of high-z quasars ever undertaken. The quasar sample is summarised in Table 1.1.

1.3 PARAMETERIC MODEL FITS

In this section we describe how parameters of the [O III] emission are derived. We employ two complementary approaches. The first approach involves the fitting of a parameteric model consisting of an empirical Fe II template and multiple Gaussian components to model the emission from the broad and narrow components of Hβ and the

Table 1.1: The numbers of quasars with [O III] line measurements and the spectrographs and telescopes used to obtain the near-infrared spectra.

Spectrograph	Telescope	Number
FIRE	MAGELLAN	32
GNIRS	GEMINI-N	29
ISAAC	VLT	6
LIRIS	WHT	5
NIRI	GEMINI-N	29
NIRSPEC	Keck II	3
SINFONI	VLT	76
SOFI	NTT	78
TRIPLESPEC	ARC-3.5m	27
TRIPLESPEC	P200	46
XSHOOTER	VLT	24
		144

[O III] doublet. This is an approach which is commonly adopted in the literature.

The second approach we adopt involves optimising the weights of ten spectral components derived from an independent component analysis (ICA) of a large sample of lower-redshift AGN with SDSS spectra covering the same spectral region.

1.3.1 *Approach One*

The spectra are first transformed in to the quasar rest-frame. The redshift used in this transformation is either derived from a multi-component Gaussian fit to the broad Hα emission ($\sim$ 40 per cent of our sample) or, when this is not possible, from a preliminary fit to the broad Hβ emission ($\sim$ 40 per cent) or narrow [O III] emission (20 per cent). However, the accuracy required of the redshift used in this transformation is only $\sim$ 1000km s^{-1}. In later sections, measures of emission line velocity shifts will be made using more accurate systemic redshift estimates derived from, for example, our parameteric model fits to the core [O III] emission.

We fit a combination of a power-law continuum and an optical Fe II template – taken from Boroson and Green, (1992) – to two windows at 4435-4700 and 5100-5535 Å. The Fe II template is convolved with a Gaussian, and the width of this Gaussian, along with the normalisation and velocity offset of the Fe II template, are free variables in the pseudo-continuum fit. As highlighted by Netzer et al., (2004), there is a prominent Fe II emission feature just redward of [O III]λ5007. Accu-

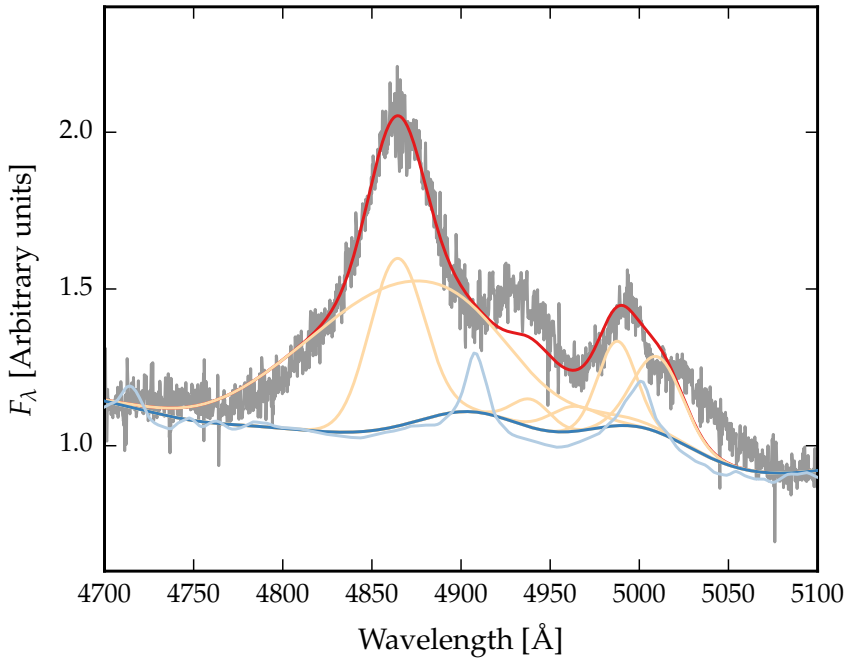

Figure 1.1: Example where poorly subtracting the iron can be confused with [O III].

rately modelling and subtracting this emission is important, because failure to do so will lead to large errors in the inferred [O III] line parameters. However, the relative strengths of the Fe II lines can differ significantly from those of I Zw 1 on which the Fe II template is based.

An example of this is shown in Fig. 1.1. Fitting the power-law+Fe II subtracted spectrum with the Gaussian model leads to a very broad and redshifted total [O III] emission profile. It's difficult to definitely rule out the origin of the emission as very broad and redshifted [O III] emission, but a much more likely scenario is that this is excess Fe II emission which is poorly modelled by the empirical template that we employ. In a later section we demonstrate how this spectrum can be extremely well fit by the ICA components with very little contribution from [O III]. .

Estimate what fraction of quasars are so affected - look at OIII flag

The following model is then fit to the spectra in the wavelength interval 4700-5100 Å. The fit is done as a function of the Doppler velocity shift, and we adopt the wavelength 4862.721Å (the laboratory Hβ wavelength) to transform wavelengths into equivalent Doppler velocities.

Hβ is modelled by two Gaussians with non-negative amplitudes and FWHM greater than 1200km s^{-1}. A handful we fix the centroids of the two Gaussians to be the same, normally because of very low S/N or because the blue wing is below the lower wavelength limit of the spectrograph. Any contribution to the Hβ emission from the

narrow-line region is weak in the vast majority of our sample, and so we do not include an additional Gaussian component to model this emission. Note: we do in fact include narrow components for eight objects in our sample. Although, for some objects, this could bias our estimate of the velocity-width of the broad component, this information is not used in the analysis presented in this paper.

Each component of the [O III] doublet is fit with one or two Gaussians, depending on the fractional reduced χ^2 difference between the one- and two-component models. If the addition of the second Gaussian decreases the reduced χ^2 by more than 5 per cent then the double-Gaussian model is accepted. One hundred and twenty-five are fit with a single Gaussian, 147 with two Gaussians, and [O III] is undetected in a further 78 quasars. When a single Gaussian is used to model each line, the peak flux ratio of the [O III] 4960 Å and 5008Å components are fixed at the expected 1:3 ratio and the width and velocity offsets are set to be equal. In the double Gaussian fit, the peak flux ratio of the second components is again fixed at 1:3, and the width and velocity offsets are again set to be equal.

In six quasars a significantly better fit was obtained by allowing the flux ratio between the two components to vary. In these quasars the best-fitting peak ratio varies from 0.50 to 0.84, with mean 0.70. **Check ICA component fits to see if this looks real.**

Model parameters were derived using a standard variance-weighted least-squares minimisation procedure employing the Levenberg-Marquardt algorithm. Prior to the fit, the spectra were inspected visually and regions significantly affected by telluric absorption or of low S/N were masked out.

However, the fits aren't always good. How to be quantative about this? Chi-squared values indicating bad fits? Also the fact that we sometimes model Fe as OIII. Discuss the limitations of using the Boroson & Greene template? Even if don't use results, should discuss Gaussian fits and their limitations, because that's what most people will be using.

It is artifical to decompose the [O III] profile in to core and wing using two Gaussians. No theoretical justification that the wing compoent should have a Gaussian profile. And decomposition depends on S/N, spectral resolution. Instead we use non-parameteric measures from the whole profile.

1.3.2 *Approach Two: Independent Component Analysis*

Independent component analysis (ICA) is a blind source separatation tecnique for separating a signal in to linearly mixed statistically independent subcomponents. Unlike the more widely-used principle component ananlysis technique, ICA produces non-negative components which allows for a physical interpretation of the components

and weights. ICA has been succesfully applied to model the spectra of emission-line galaxies (Allen et al., 2013) and BAL quasars (Allen et al., 2011). The quasar spectra can be thought of as a set of observations, $\mathbf{x}$, which are made up of statistically independent components, $\mathbf{c}$, that are combined by some mixing matric, $\boldsymbol{W}$:

$$\mathbf{x} = \boldsymbol{W}\mathbf{c} \tag{1.1}$$

ICA reverses this proces and describes how the observed data are generated. Both the independent components and the mixing matrix are unknown, but can be gound by solving:

$$\mathbf{c} = \boldsymbol{W}^{-1}\mathbf{x}. \tag{1.2}$$

Ask Paul for details.

The components were solved for using a sample of 2,154 SDSS quasars at redshifts XX. At these redshifts the SDSS spectrograph covers the rest-frame region XX-XXÅwhere Hβ and [O III] lie. The individual spectra were first adjusted to give the same overall shape as a model quasar template spectrum. Six positive independent components and four additional components that could be negative were found to be sufficient to reconstruct the spectrum, without overfitting. Each quasar spectrum can then be represented as a linear combination of the independent components:

$$x_j = \sum_{i=1}^{10} c_{ij} W_{ij} \tag{1.3}$$

For each quasar in our NIR sample perform a variance-weighted least-squares minimisation to determine the optimum value of the components weights. A power-law was fit to the quasar template spectrum in emission line free windows at 4200-4230, 4435-4700 and 5100-5535 Å. Each of the components is then divided by the power-law. An identical process is performed on each of the spectrum to be fitted, so that there is essentially zero shape in both the components and the spectrum to be fitted.

We do a preliminary fit. First six components constrained to have positive weights. Focussing on the region around [O III] (4980-5035Å), we shift the model from -10 to 10Åin jumps of 1Å. Taking the shift with the minimum chi-sqaured value, we then re-do the fit, solving again for the shift and for the component weights. This procedure ensures that the global minimum of the chi-squared distribution is reached. Good fits were achieved for 334 out of the 358 spectra.

An example is shown in Fig. 1.2.

Although the ICA is analysis is not based on any physics, there appears to be a direct correspondence between the individual components and the different emission features which contribute to the

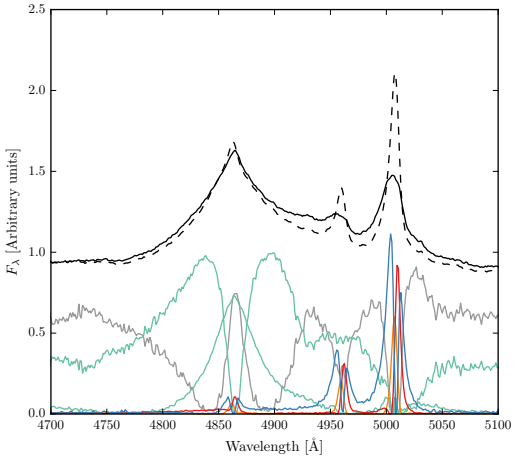

Figure 1.2: Black solid line is the median from the ICA fits to the high-luminosity sample. Black dashed line shows the median from the low-luminosity sample. The six positive ICA components are also shown.

Table 1.2: Approximate physical origin of the ICA components.

Component	Origin
w_1	Fe II
w_2	Hβ
w_3	Hβ
w_4	[O III] core
w_5	[O III] core
w_6	[O III] wing

spectra (Fig. 1.2). This correspondence is summarised in Table 1.2. The component w_1 seems to correspond to Fe II emission, the components w_2 and w_3 to broad Hβ emission, the components w_4 and w_5 to narrow [O III] emission at the systemic redshift, and the component w_6 to broad, blueshifted [O III] emission.

1.3.3 *Bad ICA fits*

There are 24 cases where the the ICA components are unable to reproduce the quasar spectrum. These are normally when we have very broad [O III]. These are clearly lacking in any significant number in the low redshift sample used to generate the ICA components. Coatman et al., (2017)

Looked at distribution of OIII strength. Excluded objects below cut. Then also exclude S/N based on simulations Reconstruct high S/N spectrum using MFICA components Then degrade S/N: Take typical noise spectrum for each instrument and add a scaled version of this.

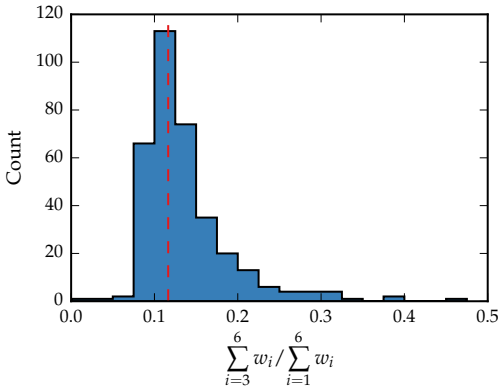

Figure 1.3: Anything to the left of the line [O III] is too weak to derive paramters from Gaussian fits. Excludes 148 objects.

Simulate 500 trials for each S/N level. Take median and 68% as the measurement and its error

1.3.4 *Derived Parameters*

All [O III] line properties are derived from the [O III]5008 emission, but, as described below, the kinematics of the peak at 4960Å are constrained by our fitting routine to be identical.

We do not to attach any physical meaning to the individual Gaussian components used in the model. While it is true that in some quasars the [O III] emission can be clearly separated in to a narrow component at the systemic redshift and a lower-amplitude, blueshifted broad component (e.g. Shen, 2016), often this decomposition is highly uncertain. Furthermore, often the S/N is not sufficient to statistically justify the addition of a second Gaussian component. Instead, we characterize the [O III] line profile using a number of non-parameteric measures, which are commonly used in the literature (e.g. Zakamska and Greene, 2014; Zakamska et al., 2016). A normalised cumulative velocity distibution is constructed from the best-fitting model, from which the velocities below which 5, 10, 25, 50, 75, 90, and 95 per cent of the total flux accumulates can be read off. The width of the emission line can then be defined, for example, using $w_{80} = v_{90} - v_{10}$. The absolute assymetry in the line profile A is defined as $((v_{95} - v_{50}) - (v_{50} - v_5))/(v_{95} - v_5)$ (Zakamska and Greene, 2014).

We also define the blueshift of the [O III] emission, which is a measure of the velocity shift of the profile from the expected position. This requires a measure of the observed line position, and an accurate measurement of the quasar systemic redshift. We use v_{10} to mesaure the location of the [O III] emission. Note that v_{50} is not suitable because when [O III] is low S/N we fit with single Gaussian.

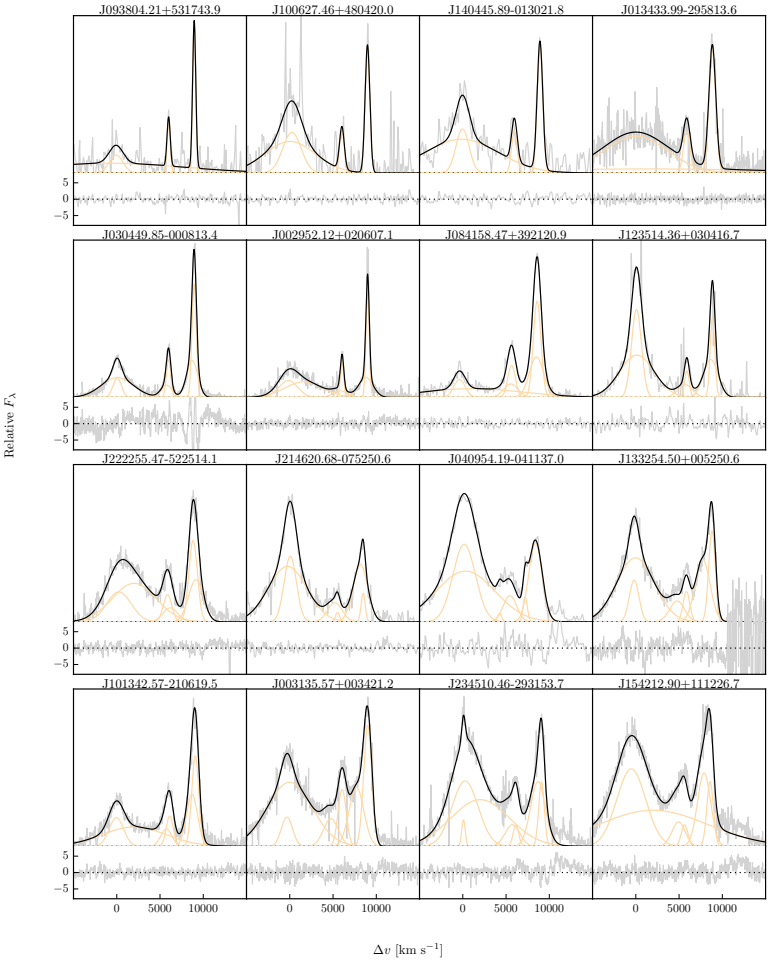

Figure 1.4: Multi-component Gaussian fits to the continuum-subtracted Hβ/[O III] emission in 16 quasars, chosen to be the representative of the wide range of [O III] line widths we measure in our sample. The data is shown in grey, the best-fitting parametric model in black, and the individual model components in orange. The broad Hβ centroid is used to measure the systemic redshift, and Δv is the velocity shift from the line rest-frame transition wavelength for Hβ. Below each fit we plot the data minus model residuals, scaled by the errors on the fluxes. **Resample model at higher resolution.**

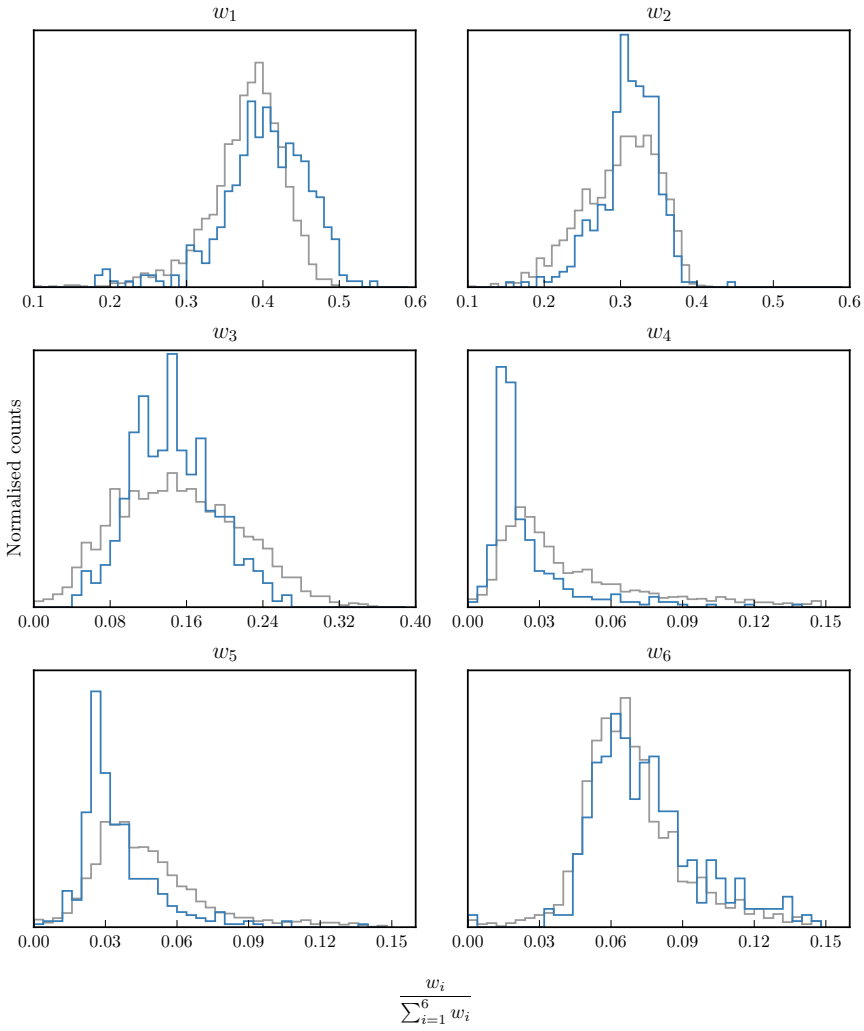

Figure 1.5: The relative weight in each of the six positive ICA components for the high-luminosity (blue) and low luminosity samples (grey). In the high-luminosity sample Fe II emission is stronger (component w_1). The core [O III] emission is weaker (components w_4, w_5) but the strength of the blueshifted wing is the same (w_6).

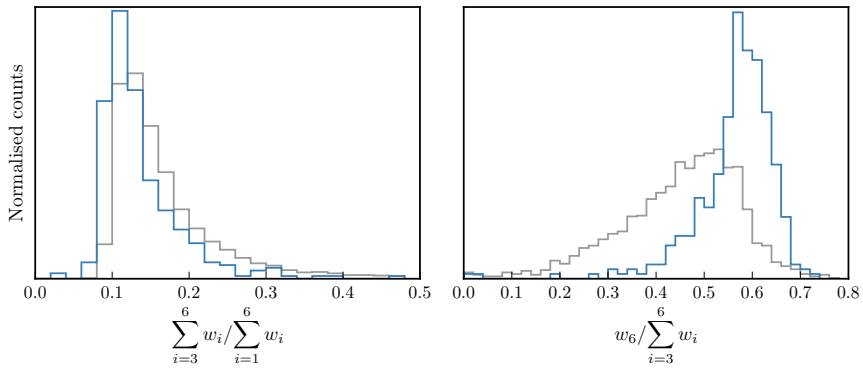

Figure 1.6: The relative weight in the three ICA components corresponding to [O III] emission (*left*) and the relative weight of the component most closely related to blueshifted [O III] emission relative to all three [O III] components (*right*). [O III] emission is weaker in the high-luminosity sample, but the relative contribution but the fractional contribution from the blueshifted component to the total [O III] emission is higher. Hence [O III] is weaker, broader, and more asymmetric in the high-luminosity sample. See Zakamska discussion.

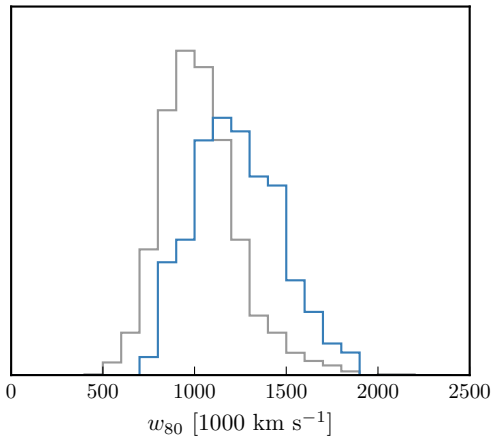

Figure 1.7: Comparison of [O III] velocity-widths in the high and low luminosity samples using the ICA component fits. If keep this need to explain in text how w_{80} is calculated from ICA component fits.

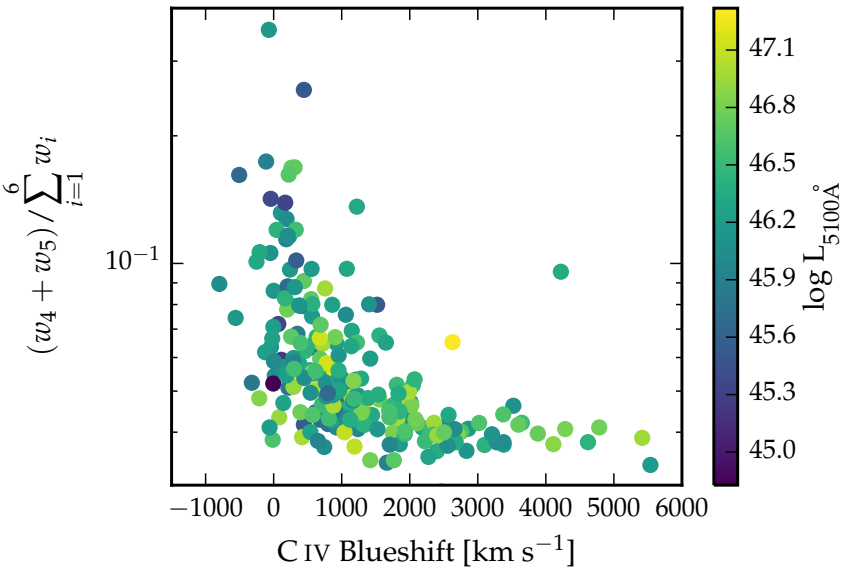

Figure 1.8: [O III] strength decreases as the C IV blueshift increases, I run in to problems comparing the C IV blueshift to the [O III] blueshift / velocity-width. See similar thing if I use [O III] EQW instead. Need to fix y ticks. Only showing the core components here. The C IV blueshift is now measured relative to the NIR ICA redshift. I think this is trend is mostly being driven by the Eigenvector 1 correlations: as the blueshift increases the Fe II strength increases and the [O III] strength decreases. Doesn't appear to be driven by the luminositiy. Is this tighter than EV1 trend shown with Fe/OIII strength by other authors? Is the AGN NLR absent in objects where outflows have reached kiloparsec scales, sweeping up the low-density material responsible for the [OIII]-emission?

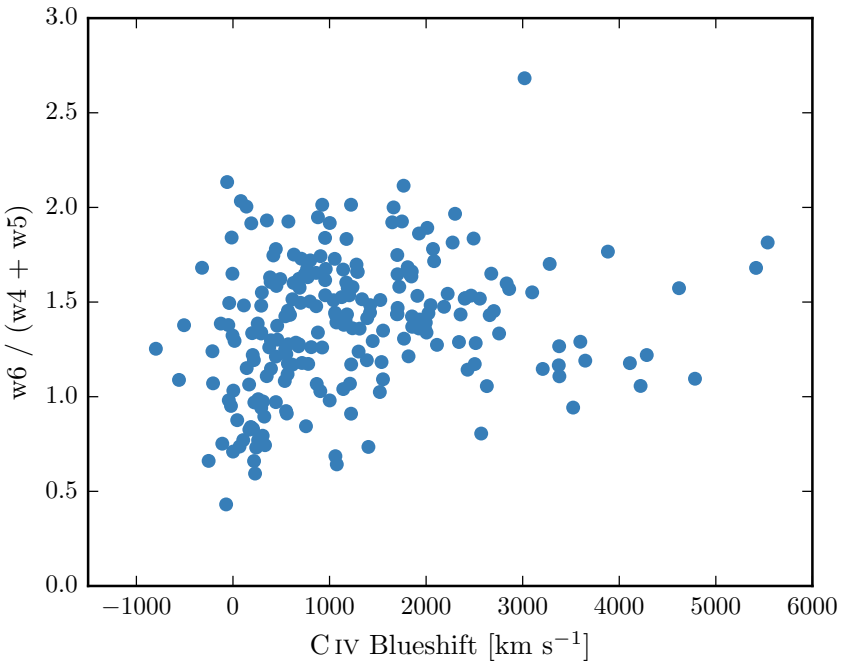

Figure 1.9: I think there is a trend here but at high blueshifts the OIII is undetected / very low S/N. Need to determin when we can believe OIII paramters. Why at low CIV blueshift is there a much bigger dynamic range than in [O III] blueshifts in Fig. 13. Is it just because we have more objects?

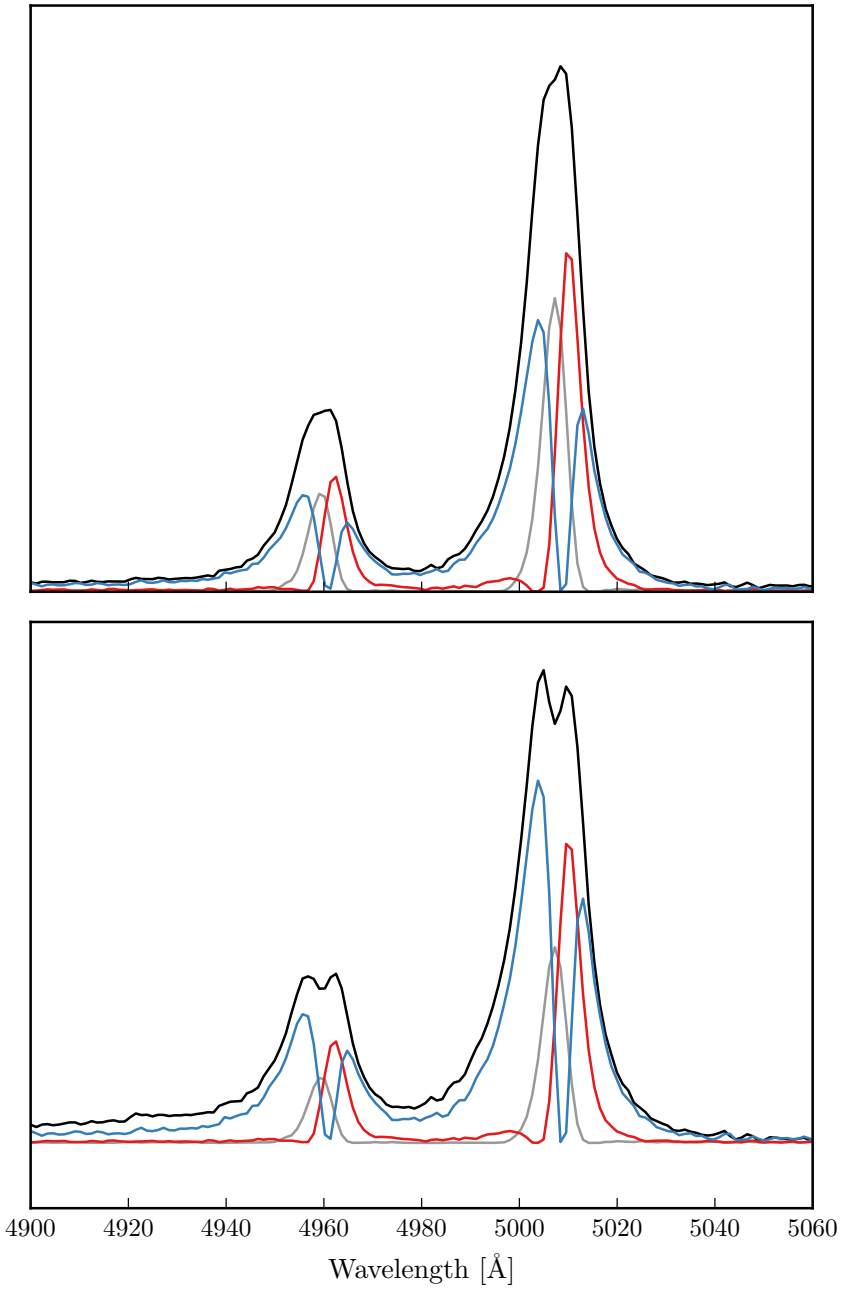

Figure 1.10: Comparison of median [O III] profiles from ICA fits it low- and high-luminosity samples.

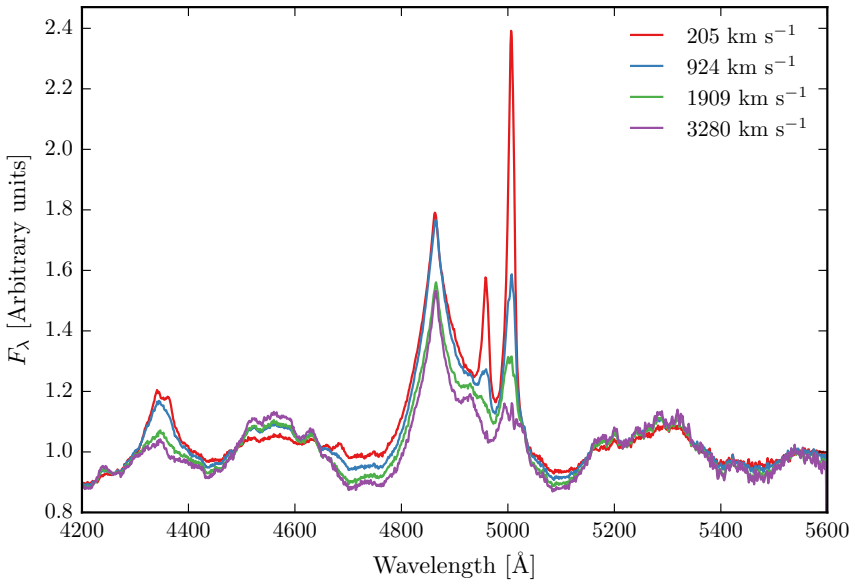

Figure 1.11: ICA median weights as a functino of the CIV blueshift.

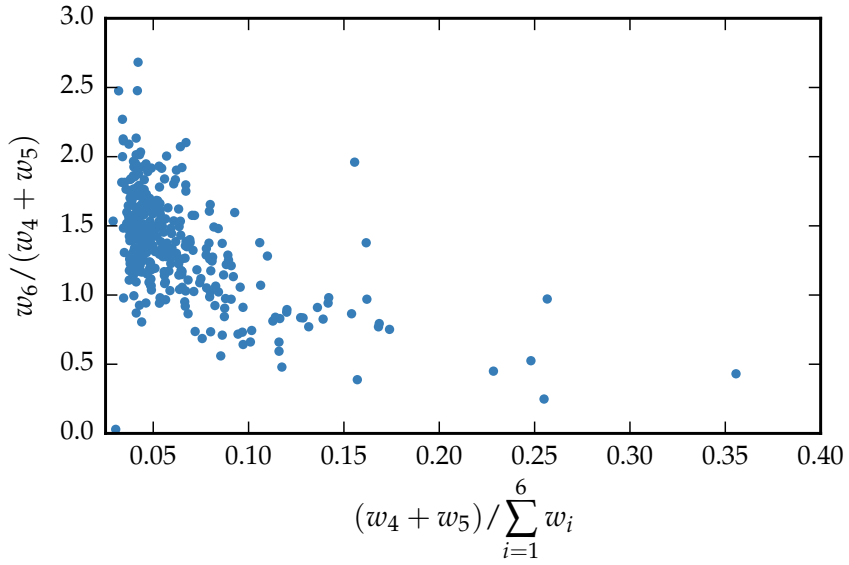

Figure 1.12: Zhang et al. 2011: Blueshift of [O III] correlates significantly with the EQW of the core. The more the peak of the line is blueshifted, the more the core component decreases dramatically, while the blue wing changes much less. We see this clearly. This is similar to behaviour of C IV? I.e. is there a mapping from this to the C IV space diagram? This would suggests that the mechamism producing the two corerlations is the same. Consistent with the core coming from the canonical extended NLR where the gas is dominate by gravity of the bulge while the wing arises in an outflow. And C IV explained by wind. Suggests intimate connection between BLR and NLR.

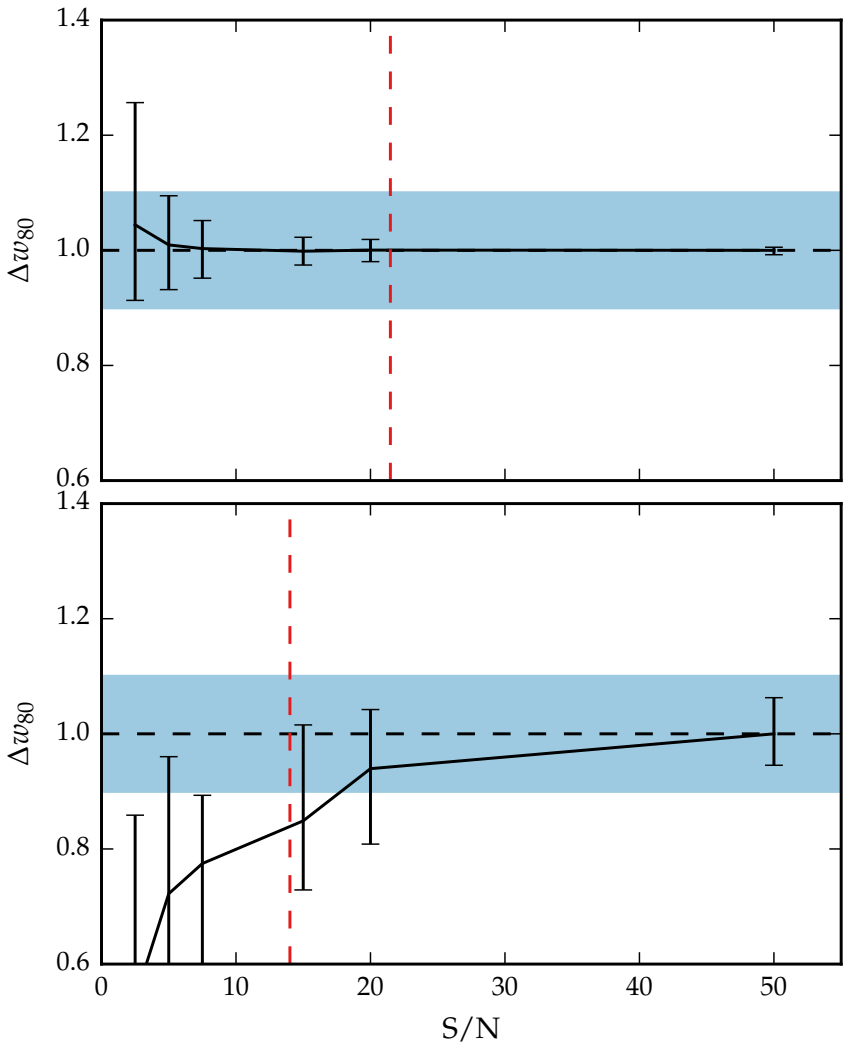

Figure 1.13

The line width measures are not at present corrected for instrumental broadening, but this can easily be done.

1.3.5 *Other flags*

Flag 2

Low S/N. Includes some of the strong iron emitters.

Flag 3

74 objects where [O III] is undetected, although I don't have a rigorous definition of what this means. Merge with 2? Section on deriving upper limits.

1.4 ICA COMPONENT FITS

What is the segue here? Sometimes Gaussians give poor fit? Not clear what is Hb, what is OIII, what is Fe? Show some examples of when the multi-Gaussian fits fail. Need to describe sample used in ICA component decomposition and briefly describe method (or refer to Allen & Hewett).

1.5 MEASURING THE QUASAR SYSTEMIC REDSHIFT

Explain flags Need to send paul redshifts

1.5.1 *Hα*

There are 224 quasars in our sample with spectra covering the Hα emission line. We discard seven of these from our sample because of very low S/N (<2.5 measured in the Hα line), leaving 217 To measure the position of the line we fit a parameteric model, which is very similar to the model described in Paper I. The continuum emission is first modeled and subtracted using the procedure described in Paper I. We then test five different models with increasing degrees of freedom to model the Hα emission. The model we select is the simplest model for which the fractional change in the reduced chi-squared from the model with the lowest reduced chi-squared is less than ten per cent.

The models we test are: (1) a single broad Gaussian; (2) two broad Gaussians with identical velocity centroids; (3) two broad Gaussians with different velocity centroids; (4) two broad Gaussians with identical velocity centroids, and additional narrower Gaussians to model the narrow Hα emission, and the narrow components of [N II]λλ6548,6584 and [S II]λλ6717,6731; (5) two broad Gaussians with different velocity centroids, and additional narrower Gaussians. If used, the width and velocity of all narrow components are set to be equal in the fit, and the relative flux ratio of the two [N II] components is fixed at the expected value of 2.96. The number of quasars fit by each model is: model 1 - 10; model 2 - 71; model 3 - 32; model 4 - 51; model 5 - 53. The redshift is then measured at the peak flux of the Hα model, including both the broad and narrow components of Hα if appropriate.

1.5.2 *ICA*

The only sensible way to measure the systemic redshift is using the NIR ICA fit. Hα and Hβ seem to give no systematic offset but large scatter, and they are often asymmetric, so should only use peak. And Hα isn't always available, and have other narrow components need to

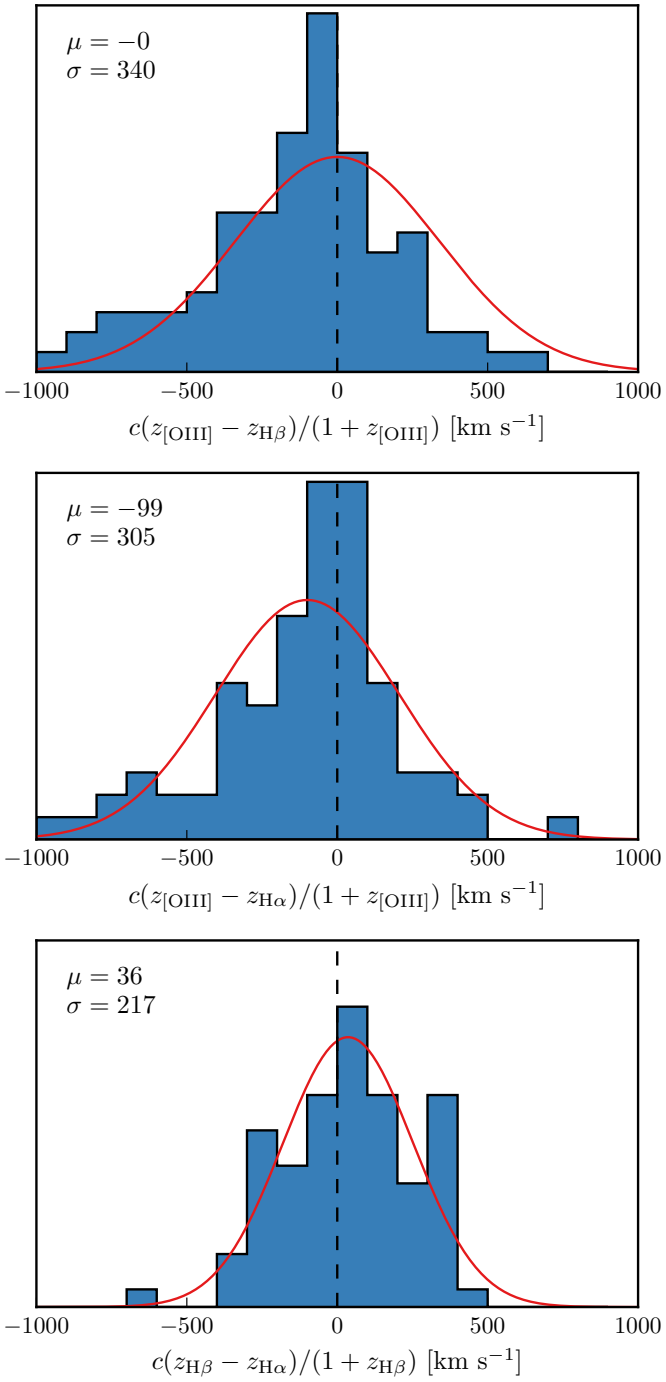

Figure 1.14: Redshift comparisons. Lots have been excluded from Ha/Hb so need to look at flags greater than one. What is the big peak? Gaussian fit to the first one has failed. Find out why these plots look different to ones in paper.

decompose. O III peak is mostly fine to use, but then there are some objects where the whole line is blueshifted. And critically, at large CIV blueshifts the [O III] emission is often undetected. Can show comparison of NIR ICA redshifts to... Optical ICA? Hewett & Wild?

Should emphasise that most people use [O III] to get the most reliable systemic redshift. While this is fine at low luminosities, at high luminosities this can result in large errors (profile can be dominated by blueshifted component, Fe emission can be improperly subtracted, or [O III] might not be detected at all. Publish ICA components with this paper?

Can also describe what I found trying to get redshifts from broad Hα, Hβ? (Narrow components generally very weak at these luminosities so can't be used.) Generally find no systematic errors but large ($\sim$1000km s^{-1} scatter). Comparing NIR ICA to [O III] for the [O III] with high S/N I find small (few hundred km s^{-1}) scatter.

Should publish [O III] redshifts with this paper for people to use.

1.5.3 *Parameter uncertainties and upper limits*

Describe how uncertainties on best-fitting parameters were calculated.

In 78 quasars, or approximately 25 per cent of or sample, the [O III] is undetected, or detected with very low S/N. In this section we describe how upper limits on the [O III] equivalent width were calculated. Firstly, the best-fitting model comprising the continuum, Fe II, and Hβ emission is subtracted from the spectra, leaving behind only emission due to [O III]. From this spectra we generate 100 mock spectra, where the flux at each wavelength is randomly drawn from a Normal distribution with a mean equal to the flux convolved with a Gaussian of width 200km s^{-1}and a width equal to the known error. We then perform an error-weighted linear least-squares regression with an [O III] template derived from a fit to a very high S/N low redshift SDSS composite spectra. The equivalent width of the best-fitting model is recorded for each of the 100 realisations of the spectra. The error in the equivalent width is defined as the root-mean-square of these values.

Calculated uncertainties using Monte Carlo. Uncertainties on v10 are very large, which I think makes sense since the wing Gaussian will be appearing and disappering, giving a large dispersion in v10. Or regardles v10 is just very sensitive to the noise. Maybe I should be using v25 instead?

1.5.4 *Absolute flux calibration of spectra and continuum luminosities*

Relative flux-calibration of the infrared spectra as a function of wavelength has been achieved, to $\simeq$10 per cent, through observations of

appropriate flux standards. The absolute flux levels, however, can be in error by large factors due to variable atmospheric conditions combined with the narrow slit widths. For the majority of the quasars we have, therefore, established the absolute flux scale for each near-infrared spectrum using the same quasar SED-model fitting scheme employed in Paper I. Briefly, the SED-model was fit, with the normalisation and E(B-V) as free varibales, to optical/infrared magnitudes, or SDSS/BOSS spectra (check order I do this.) This allows us to extrapolate from the optical when we do not have photometric data in the near-infrared. The spectra were then normalised to the SED model using a linear error-weighted least-squares regression in the the regions of the spectra covered by the H/K bands. The monochromatic continuum luminosity at 5100Åwas calculated directly from the normalised SED-model. **If this sounds strange can also calculate from fit to normaised spectra. Check if any missing normalisation / monochromatic luminosities.**

1.6 RESULTS FROM ICA FITS

Need to convince the reader that the ICA components approximately correspond to real components. Explain how non-parameteric measures derived form ICA reconstructions.

We find there is a decreasing symmetric component at high luminosities. Relates directly to Shen and Ho, (2014). A stable narrow line region is removed by the outflowing material. Shen and Ho, (2014) showed that the strength of the core [O III] component decreases with quasar luminosity and optical Fe II strength faster than the wing component, leading to overall broader and more blueshifted profiles as luminoisty and Fe II strength (or C IV blueshift) increases.

1.7 LUMINOSITY/REDSHIFT-EVOLUTION OF [O III] PROPERTIES

In this section we look for any luminosity/redshift dependent changes in the [O III] line properties. To do this we extend the dynamic range of our samples in terms of both luminosity and redshift by supplementing our sample with quasars presented by Zakamska and Greene, (2014) and Harrison et al., (2016).

The Zakamska and Greene, (2014) objects are a sample of 568 obscured luminous quasars selected from SDSS (Reyes et al., 2008; Yuan, Strauss, and Zakamska, 2016). They are selected to have [O III] luminosities above $10^{8.5}L_{\odot}$ and have a median redshift $z = 0.397$.

We also include 40 quasars at redshifts $1.1 \leqslant z \leqslant 1.7$) from the KMOS AGN Survey at High redshift (KASHz) with [O III] line measurements.

We also have the same information for ~20 000 SDSS spectra from Mullaney et al., (2013).

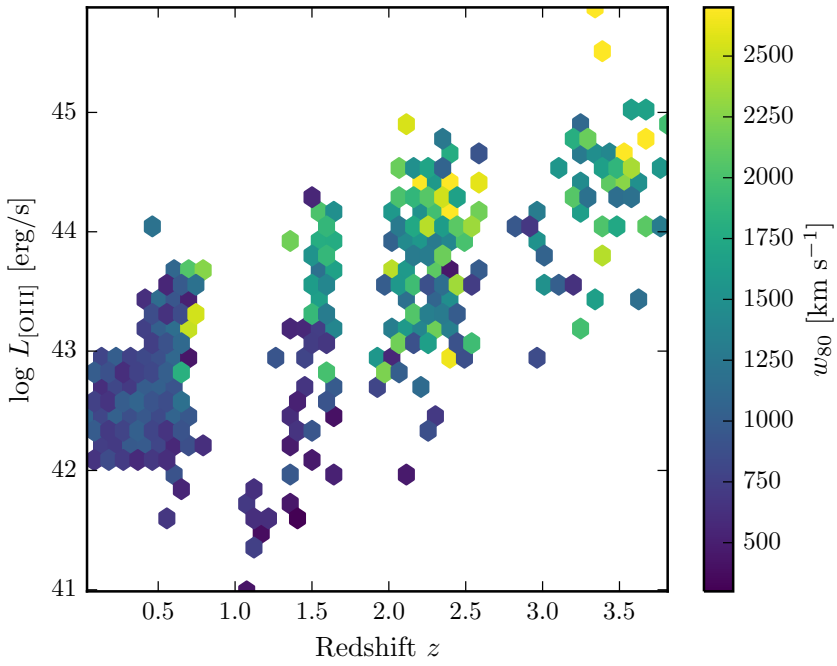

Figure 1.15: The [O III] velocity-width, characterised by w_{80}, as a function the [O III] luminosity and the quasar redshift. The color of each hexagon denotes the mean w_{80} for the obects in that luminosity-redshift bin. We have suplemented our sample with low-z objects from Zakamska and Greene, (2014) and medium ($z \sim 1.5$) redshift objects from Harrison et al., (2016). If I keep this plot make sure its clear which points belong to which sample.

In Figure 1.15 we show the [O III] velocity width as a function of the [O III] luminosity and the quasar redshift. The lack of any redshift-evolution between $z = 0$ and $z = 1.5$ was reported by Harrison et al., (2016). Our additional data suggets that this continues to $z \sim 2.5$. On the other hand, at fixed redshift, we see a significant correlation between the [O III] velocity width and the luminosity.

The fact that we don't see many broad lines in the Zakamska and Greene, (2014) objects even at luminosities >43 erg/s could be due to the fact that these are all type II quasars, whereas the sample presented in this paper are all type I. Mullaney et al., (2013) showed that the [O III] lines of type I quasars are typically broader than in type II quasars.

Looking at the [O III] velocity width as a function of luminosity tells us about the physical drivers of the outflows observed in [O III]. The correlation with luminosity suggests that the highest velocity outflows are associated with the most luminous AGN. This has been reported for low-redshift AGN, for both ionized and molecular outflows (e.g. Westmoquette et al. 2012; Veilleux et al. 2013; Arribas et al. 2014; Cicone et al. 2014; Hill & Zakamska 2014).

This suggests that the outflows are driven by radiative forces. On the other hand, Mullaney et al., (2013) find that once the correlation between the [O III] luminosity and the radio luminosity has been taken in to account, the [O III] velocity width is more strongly related to the radio luminosity of the AGN.

1.8 EQUIVALENT WIDTH

In Fig. 1.16 we show the [O III]5008 EW as a function of the quasar bolometric luminosity. Bolometric luminosity is estimated from the monochromatic continuum luminoisty at 5100Åusing the correction factor given by Richards et al., (2006). For comparison, we also show the low-z sample from Shen et al., (2011).

The equivalent width of [O III] has been found to strongly decrease as a function of redshift and/or luminosity (e.g. Brotherton, 1996; Netzer et al., 2004; Sulentic et al., 2004; Baskin and Laor, 2005).

The size of the narrow line region is roughly expected to scale as $L^{0.5}$ (e.g. Netzer et al., 2004). However, for high luminosity quasars with strong [O III] this gives NLR sizes which are unreasonably large (~100 kpc; Netzer et al., 2004).

Netzer et al., (2004) found 1/3 of their high luminosity sample had very weak [O III], whereas quasars with weak [O III] are very rare for nearby AGN. We find a very similar fraction. Netzer et al., (2004) claim that for the population of strong [O III] emitters there is no reduction of EW with increasing source luminosity. On the other hand, there are many weak or no [O III] emitters at high luminosity that

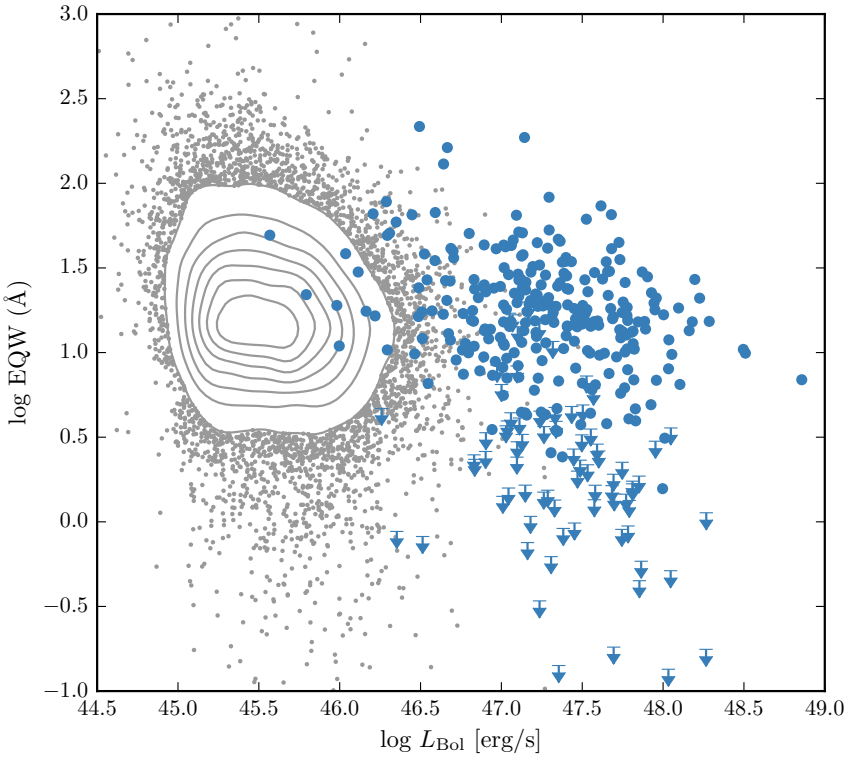

Figure 1.16: The [O III] EW as a function of the quasar bolometric luminosity for the sample presented in this paper (blue circles) and the low-z SDSS sample (grey points and contours). Upper limits are denoted by the downward arrows.

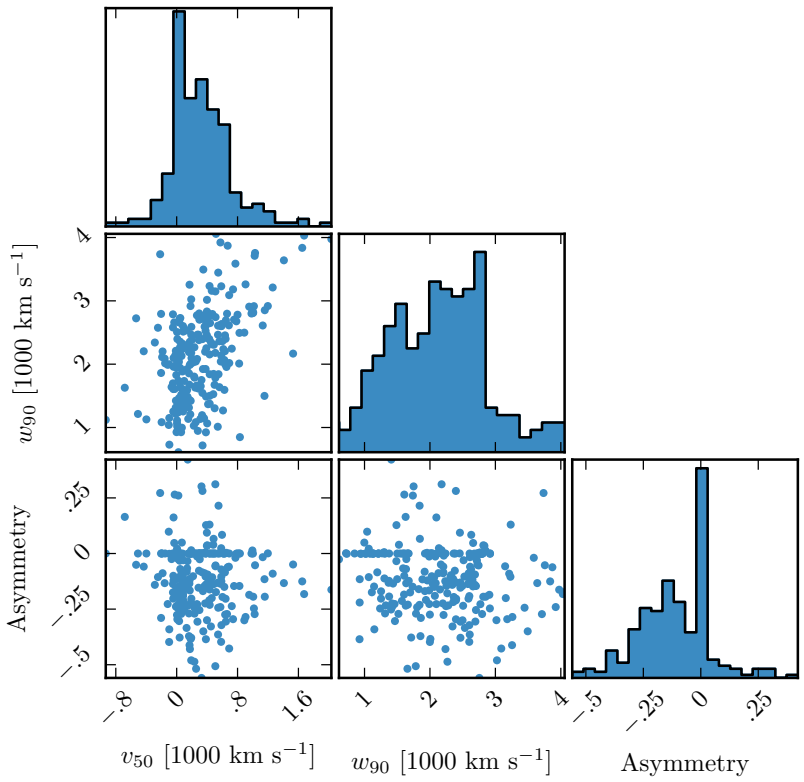

Figure 1.17: The distributions of and correlations between a subset of the non-parameteric measures we made of the best-fitting [O III] models.

could give the impression that the line EQW decreases with increasing source luminoisity.

1.8.1 *OIII outflows*

Our best-fitting profiles show a strongly blue-asymmetric profile (Fig. 1.17), with a significant fraction of the total emission in a blue wing. The luminous blueshifted broad wing and the exteremely broad profile reveals high-velocity outflowing ionized gas. This can be explained if the far-side of any outflowing gas, that is moving away from the line of sight, is obscured by dust in the host galaxies (e.g. Heckman et al. 1981; Vrtilek 1985). Observations at both low and high redshifts commonly observe this blueshifted component. Our results, and those of other authors, suggest that kpc-scale outflows in ionized gas are common among the most luminous high-redshift actively accreting SMBHs.

The situtation is very different in nearby AGN, where the [O III] velocity width is dominated by the galactic potential and correlates

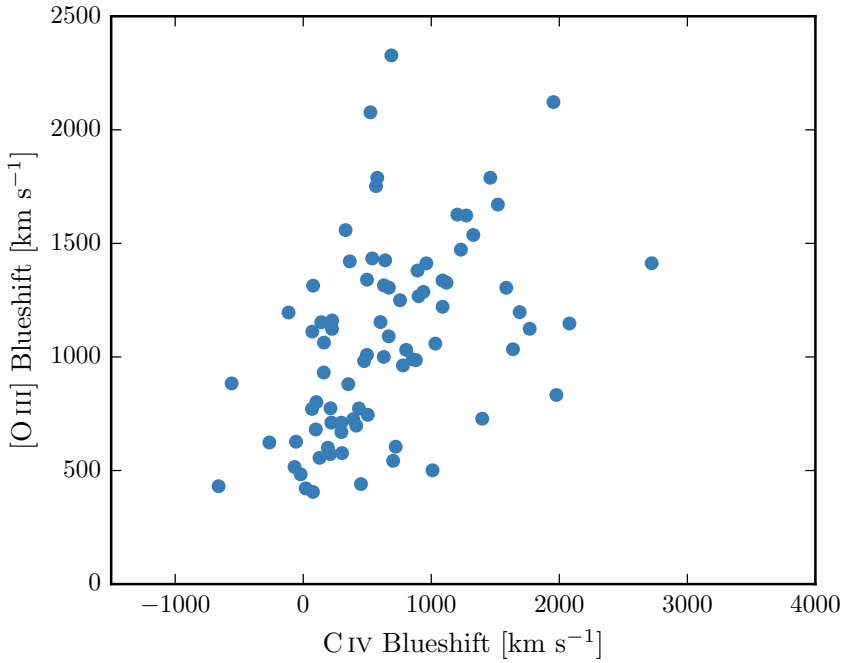

Figure 1.18: The relation between the blueshifts of C IV and [O III]. Equivalent to Fig 8. We use the Hβ peak in this figure, which I think is responsible for some of the trend. However, we do see a correlation (albeit noisier) using the NIR ICA redshifts. Not a sensible to use the [O III] redshifts, since these become much more unreliable at the high C IV blueshift end (when [O III] is weaker: figure 7. Note that we are using v_{10} for the [O III] position and v_{50} for the C IV position. We can't use v_{50} for [O III] because sometimes we are using a single Gaussian, especially if the [O III] is weaker and we miss the broad component. Need to remake this plot / don't use at all because I don't believe some of the Gaussian fits to [O III], especially at high C IV blueshifts when [O III] is weak and Fe II is strong.) Only objects where fit with two components.

well with the stellar velocity dispersion. HI, CO and absorption line mesaures of the host galaxy rest frame suggest that [O III] usually gives consistent results within 200 km/s (de Robertis 1985; Whittle 1985; Wilson & Heckman 1985; Condon et al. 1985; Stripe 1990; Alloin et al. 1992; Evans et al. 2001).

We see a correlation between the [O III] velocity width and blueshift. As the blueshift of the line increases it gets broader. This is consistent with Shen and Ho, (2014), where the strength of the narrow core is decreasing, leading to a broader and more blueshifted profile.

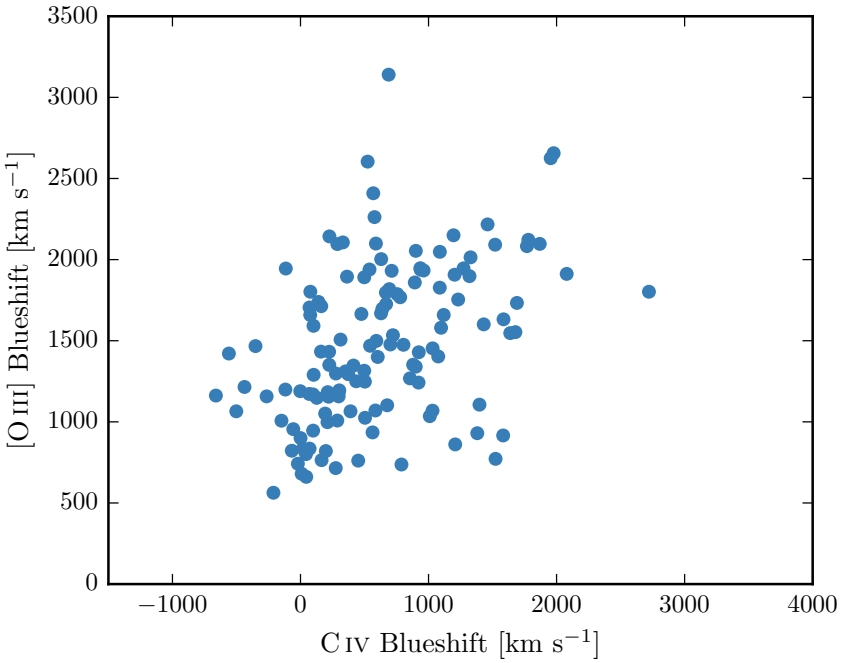

Figure 1.19

1.8.2 *[O III] and C IV outflows are linked*

As described in Paper I, we have searched for optical counterparts to our near-infrared spectra. Optical spectra are available for XXX quasars in our catalogue, and cover the broad C IV doublet. As we described in Paper I and Coatman et al., (2016), C IV is often blueshifted, which almost certainly signal the presence of strong outflows, most likely originating in a disc wind. In Paper I we demonstrated that the quasars in our sample cover the full range of C IV blueshifts seen in the SDSS quasar population, which makes our sample unique in that it allows us to study properties of the quasar across the full parameter range.

The C IV velocity centroid measurements are taken directly from paper I. We define the 'location' of the [O III] emission using v_{10}, although the results are the same if v_{20}, v_{50} etc. are used instead.

In Figure 1.18 we show the C IV blueshifts against the [O III] blueshifts. This comparison is done for a sub-sample of 146 objects where we have good measurements of the C IV, [O III], and Hβ (to measure the systemic redshift) profiles. Objects with S/N > 3 are shown as blue filled circles and objects with S/N < 3 as open grey circles. We calculated the median S/N per pixel in the best-fitting model for the [O III]5008 emission.

There is a clear and strong correlation. Similar correlations have been tentatively found in lower redshift quasars and AGN (Zamanov et al., 2002).

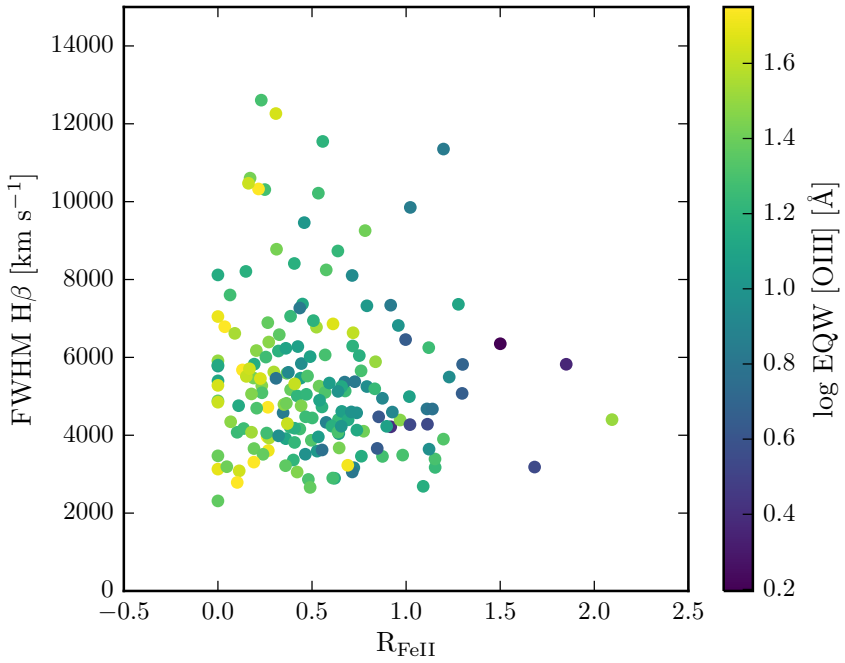

Figure 1.20: The [O III] EQW as a function of the Hβ FWHM and the optical Fe II strength (EQW Fe II/ EQW Hβ).

The blueshifting of C IV is known to correlate with luminosity (Richards et al., 2011). In [O III], the blueshifted wing becomes relatively more prominent as the luminosity of the quasar increases (Shen and Ho, 2014). Therefore, it is plausible that the correlation between the C IV and [O III] blueshifts is a secondary effect that is driven by the correlation of each with the luminosity. In Figure **??** we color the data points by the luminosity, and no luminosity-dependent trends are apparent. We find that both the [O III] and C IV blueshifts are correlated with the luminosity, but that these correlations are much weaker than the correlation between the [O III] and C IV blueshifts.

1.9 EIGENVECTOR ONE CORRELATIONS

Because of this diversity, it is the dominant variable in the set of correlations making up EV1, which is believed to be linked to certain fundamental parameters of the accretion process. In Figure 1.20 we show the [O III] EQW as a function of the Hβ FWHM and the optical Fe II strength. The optical Fe II strength is defined as the ratio of the Fe II and Hβ EQW, where the Fe II EQW is measured between 4434 and 4684Å. These parameters form part of 'eigenvector 1' (EV1), the first eigenvector in a principal component analysis which originated from the work of Boroson and Green, (1992). In our sample, these parameters follow very similar correlations to what is observed at low-z

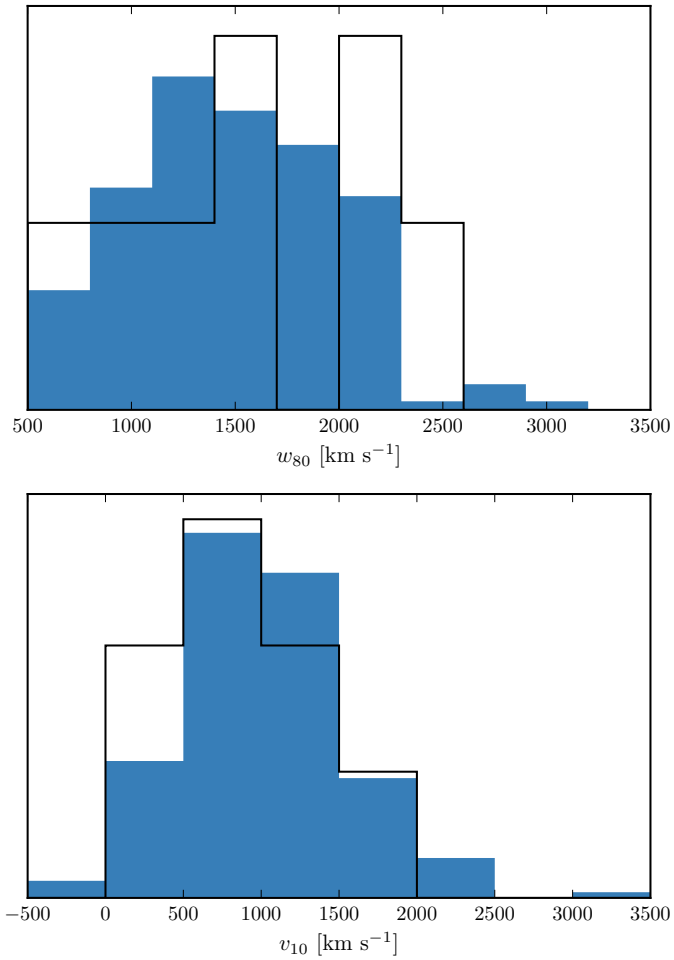

Figure 1.21: The distribution of w_{80} and v_{10} for the 19 BALs are compared to the distribution for the non-BALs. These look rubbish. Cumulative distributions instead? Try doing gaussian kernel density estimator

(e.g. Shen and Ho, 2014). In particular, the anti-correlation between the [O III] and Fe II EQWs.

Same as Shen, (2016), we confirm that the EV1 correlations hold at high luminosities/redshifts. See also Sulentic et al. 2004, 2006; Runnoe et al. 2013. Make sure it's clear that Shen, (2016) quasars make up a significant chunk of our sample.

1.10 MAPPING EV1 TO CIV BLUESHIFT AND EQW

1.11 SIGNAL TO NOISE TESTS

1.12 BROAD ABSORPTION LINE QUASARS

19 quasars in our catalogue are classified as broad absorption line (BAL) quasars, using the either the SDSS classification flags or the Allen et al., (2011) catalogue. We find that the BAL quasars have typically broader [O III] than the rest of the sample. Note that in the Zakamska et al., (2016) sample of very red quasars, the incidence of BALs is very high, and these objects have extremely broad [O III] profiles. A two-sided Kolmogorov-Smirnov statistic on the w_{80} distributions returned a p-value of 0.10. What does this mean? Try with different parameters? Histograms look rubbish so maybe just give the numbers.

1.13 DISCUSSION

1.13.1 *Type II quasars*

Implications of our findings on searches for high-redshift type 2 quasars. It could be that type II quasars exist. If you look at CIV/MgII the narrow line components are very weak. So the contribution from the narrow line region is very weak in luminous quasars, and you just won't see it even if the broad line region is obscured. Findings in this paper seem to suggest that the startic narrow line region is very weak in luminous quasars.

BIBLIOGRAPHY

Alatalo, K. et al. (2011). "Discovery of an Active Galactic Nucleus Driven Molecular Outflow in the Local Early-type Galaxy NGC 1266." In: *ApJ* 735, 88, p. 88. DOI: 10.1088/0004-637X/735/2/88. arXiv: 1104.2326.

Alexander, D. M., A. M. Swinbank, I. Smail, R. McDermid, and N. P. H. Nesvadba (2010). "Searching for evidence of energetic feedback in distant galaxies: a galaxy wide outflow in a z ~ 2 ultra-luminous infrared galaxy." In: *MNRAS* 402, pp. 2211–2220. DOI: 10.1111/j.1365-2966.2009.16046.x. arXiv: 0911.0014.

Allen, J. T., P. C. Hewett, N. Maddox, G. T. Richards, and V. Belokurov (2011). "A strong redshift dependence of the broad absorption line quasar fraction." In: *MNRAS* 410, pp. 860–884.

Allen, J. T., P. C. Hewett, C. T. Richardson, G. J. Ferland, and J. A. Baldwin (2013). "Classification and analysis of emission-line galaxies using mean field independent component analysis." In: *MNRAS* 430, pp. 3510–3536. DOI: 10.1093/mnras/stt151. arXiv: 1301.5930.

Arav, N., M. Moe, E. Costantini, K. T. Korista, C. Benn, and S. Ellison (2008). "Measuring Column Densities in Quasar Outflows: VLT Observations of QSO 2359-1241." In: *ApJ* 681, 954-964, pp. 954–964. DOI: 10.1086/588651. arXiv: 0807.0228.

Baskin, A. and A. Laor (2005). "What controls the [OIII]λ5007 line strength in active galactic nuclei?" In: *MNRAS* 358, pp. 1043–1054. DOI: 10.1111/j.1365-2966.2005.08841.x. eprint: astro-ph/0501436.

Bischetti, M. et al. (2016). "The WISSH Quasars Project I. Powerful ionised outflows in hyper-luminous quasars." In: *ArXiv e-prints*. arXiv: 1612.03728.

Boroson, T. A. and R. F. Green (1992). "The emission-line properties of low-redshift quasi-stellar objects." In: *ApJS* 80, pp. 109–135.

Boroson, T. (2005). "Blueshifted [O III] Emission: Indications of a Dynamic Narrow-Line Region." In: *AJ* 130, pp. 381–386. DOI: 10.1086/431722. eprint: astro-ph/0505127.

Brotherton, M. S. (1996). "The Profiles of H beta and [O iii] lambda 5007 in Radio-loud Quasars." In: *ApJS* 102, p. 1. DOI: 10.1086/192249. eprint: astro-ph/9507067.

Brusa, M. et al. (2015). "X-shooter reveals powerful outflows in z~1.5 X-ray selected obscured quasi-stellar objects." In: *MNRAS* 446, pp. 2394–2417. DOI: 10.1093/mnras/stu2117. arXiv: 1409.1615.

Carniani, S. et al. (2015). "Ionised outflows in z ~ 2.4 quasar host galaxies." In: *A&A* 580, A102, A102. DOI: 10.1051/0004-6361/201526557. arXiv: 1506.03096.

Cicone, C. et al. (2014). "Massive molecular outflows and evidence for AGN feedback from CO observations." In: *A&A* 562, A21, A21. DOI: 10.1051/0004-6361/201322464. arXiv: 1311.2595.

Cimatti, A., M. Brusa, M. Talia, M. Mignoli, G. Rodighiero, J. Kurk, P. Cassata, C. Halliday, A. Renzini, and E. Daddi (2013). "Active Galactic Nucleus Feedback at z ~ 2 and the Mutual Evolution of Active and Inactive Galaxies." In: *ApJ* 779, L13, p. L13. DOI: 10.1088/2041-8205/779/1/L13. arXiv: 1311.4401.

Coatman, L., P. C. Hewett, M. Banerji, and G. T. Richards (2016). "CIV emission-line properties and systematic trends in quasar black hole mass estimates." In: *MNRAS* 461, pp. 647–665. DOI: 10.1093/mnras/stw1360. arXiv: 1606.02726.

Coatman, L., P. C. Hewett, M. Banerji, G. T. Richards, J. F. Hennawi, and J. X. Prochaska (2017). "Correcting C IV-based virial black hole masses." In: *MNRAS* 465, pp. 2120–2142. DOI: 10.1093/mnras/stw2797. arXiv: 1610.08977.

Dunn, J. P., M. Bautista, N. Arav, M. Moe, K. Korista, E. Costantini, C. Benn, S. Ellison, and D. Edmonds (2010). "The Quasar Outflow Contribution to AGN Feedback: VLT Measurements of SDSS J0318-0600." In: *ApJ* 709, pp. 611–631. DOI: 10.1088/0004-637X/709/2/611. arXiv: 0911.3896.

Feldman, F. R., D. W. Weedman, V. A. Balzano, and L. W. Ramsey (1982). "Emission-line widths in galactic nuclei." In: *ApJ* 256, pp. 427–434. DOI: 10.1086/159919.

Feruglio, C., R. Maiolino, E. Piconcelli, N. Menci, H. Aussel, A. Lamastra, and F. Fiore (2010). "Quasar feedback revealed by giant molecular outflows." In: *A&A* 518, L155, p. L155. DOI: 10.1051/0004-6361/201015164. arXiv: 1006.1655.

Greene, J. E. and L. C. Ho (2005). "A Comparison of Stellar and Gaseous Kinematics in the Nuclei of Active Galaxies." In: *ApJ* 627, pp. 721–732. DOI: 10.1086/430590. eprint: astro-ph/0503675.

Greene, J. E., N. L. Zakamska, X. Liu, A. J. Barth, and L. C. Ho (2009). "The Growth of Black Holes: Insights from Obscured Active Galaxies." In: *ApJ* 702, pp. 441–459. DOI: 10.1088/0004-637X/702/1/441. arXiv: 0907.1086 [astro-ph.GA].

Greene, J. E., N. L. Zakamska, L. C. Ho, and A. J. Barth (2011). "Feedback in Luminous Obscured Quasars." In: *ApJ* 732, 9, p. 9. DOI: 10.1088/0004-637X/732/1/9. arXiv: 1102.2913.

Hainline, K. N., R. Hickox, J. E. Greene, A. D. Myers, and N. L. Zakamska (2013). "SALT Long-slit Spectroscopy of Luminous Obscured Quasars: An Upper Limit on the Size of the Narrow-line Region?" In: *ApJ* 774, 145, p. 145. DOI: 10.1088/0004-637X/774/2/145. arXiv: 1307.5852.

Harrison, C. M. et al. (2012). "Energetic galaxy-wide outflows in high-redshift ultraluminous infrared galaxies hosting AGN activity." In: *MNRAS* 426, pp. 1073–1096. DOI: 10.1111/j.1365-2966.2012.21723.x. arXiv: 1205.1801.

Harrison, C. M., D. M. Alexander, J. R. Mullaney, and A. M. Swinbank (2014). "Kiloparsec-scale outflows are prevalent among luminous AGN: outflows and feedback in the context of the overall AGN population." In: *MNRAS* 441, pp. 3306–3347. DOI: 10.1093/mnras/stu515. arXiv: 1403.3086.

Harrison, C. M., D. M. Alexander, J. R. Mullaney, J. P. Stott, A. M. Swinbank, V. Arumugam, F. E. Bauer, R. G. Bower, A. J. Bunker, and R. M. Sharples (2016). "The KMOS AGN Survey at High redshift (KASHz): the prevalence and drivers of ionized outflows in the host galaxies of X-ray AGN." In: *MNRAS* 456, pp. 1195–1220. DOI: 10.1093/mnras/stv2727.

Heckman, T. M., G. K. Miley, and R. F. Green (1984). "The kinematics of the narrow-line region in active galaxies and quasars. III - Correlations with the broad-line region and radio emission." In: *ApJ* 281, pp. 525–534. DOI: 10.1086/162125.

Heckman, T. M., G. K. Miley, W. J. M. van Breugel, and H. R. Butcher (1981). "Emission-line profiles and kinematics of the narrow-line region in Seyfert and radio galaxies." In: *ApJ* 247, pp. 403–418. DOI: 10.1086/159050.

Kim, M., L. C. Ho, C. J. Lonsdale, M. Lacy, A. W. Blain, and A. E. Kimball (2013). "Evidence for Active Galactic Nucleus Driven Outflows in Young Radio Quasars." In: *ApJ* 768, L9, p. L9. DOI: 10.1088/2041-8205/768/1/L9. arXiv: 1303.7194.

Moe, M., N. Arav, M. A. Bautista, and K. T. Korista (2009). "Quasar Outflow Contribution to AGN Feedback: Observations of QSO SDSS J0838+2955." In: *ApJ* 706, pp. 525–534. DOI: 10.1088/0004-637X/706/1/525. arXiv: 0911.3332.

Mullaney, J. R., D. M. Alexander, S. Fine, A. D. Goulding, C. M. Harrison, and R. C. Hickox (2013). "Narrow-line region gas kinematics of 24 264 optically selected AGN: the radio connection." In: *MNRAS* 433, pp. 622–638. DOI: 10.1093/mnras/stt751. arXiv: 1305.0263.

Nardini, E. et al. (2015). "Black hole feedback in the luminous quasar PDS 456." In: *Science* 347, pp. 860–863. DOI: 10.1126/science.1259202. arXiv: 1502.06636 [astro-ph.HE].

Nesvadba, N. P. H., M. D. Lehnert, F. Eisenhauer, A. Gilbert, M. Tecza, and R. Abuter (2006). "Extreme Gas Kinematics in the z=2.2 Powerful Radio Galaxy MRC 1138-262: Evidence for Efficient Active Galactic Nucleus Feedback in the Early Universe?" In: *ApJ* 650, pp. 693–705. DOI: 10.1086/507266. eprint: astro-ph/0606530.

Nesvadba, N. P. H., M. D. Lehnert, C. De Breuck, A. M. Gilbert, and W. van Breugel (2008). "Evidence for powerful AGN winds at high

redshift: dynamics of galactic outflows in radio galaxies during the "Quasar Era"." In: *A&A* 491, pp. 407–424. DOI: 10.1051/0004-6361:200810346. arXiv: 0809.5171.

Nesvadba, N. P. H., F. Boulanger, P. Salomé, P. Guillard, M. D. Lehnert, P. Ogle, P. Appleton, E. Falgarone, and G. Pineau Des Forets (2010). "Energetics of the molecular gas in the H_2 luminous radio galaxy 3C 326: Evidence for negative AGN feedback." In: *A&A* 521, A65, A65. DOI: 10.1051/0004-6361/200913333. arXiv: 1003.3449.

Netzer, H., O. Shemmer, R. Maiolino, E. Oliva, S. Croom, E. Corbett, and L. di Fabrizio (2004). "Near-Infrared Spectroscopy of High-Redshift Active Galactic Nuclei. II. Disappearing Narrow-Line Regions and the Role of Accretion." In: *ApJ* 614, pp. 558–567. DOI: 10.1086/423608. eprint: astro-ph/0406560.

Perna, M. et al. (2015). "Galaxy-wide outflows in z ~ 1.5 luminous obscured quasars revealed through near-IR slit-resolved spectroscopy." In: *A&A* 574, A82, A82. DOI: 10.1051/0004-6361/201425035. arXiv: 1410.5468.

Reyes, R., N. L. Zakamska, M. A. Strauss, J. Green, J. H. Krolik, Y. Shen, G. T. Richards, S. F. Anderson, and D. P. Schneider (2008). "Space Density of Optically Selected Type 2 Quasars." In: *AJ* 136, pp. 2373–2390. DOI: 10.1088/0004-6256/136/6/2373. arXiv: 0801.1115.

Richards, G. T. et al. (2006). "Spectral Energy Distributions and Multiwavelength Selection of Type 1 Quasars." In: *ApJS* 166, pp. 470–497.

Richards, G. T., N. E. Kruczek, S. C. Gallagher, P. B. Hall, P. C. Hewett, K. M. Leighly, R. P. Deo, R. M. Kratzer, and Y. Shen (2011). "Unification of Luminous Type 1 Quasars through CIV Emission." In: *AJ* 141, p. 167.

Rupke, D. S. N. and S. Veilleux (2013). "Breaking the Obscuring Screen: A Resolved Molecular Outflow in a Buried QSO." In: *ApJ* 775, L15, p. L15. DOI: 10.1088/2041-8205/775/1/L15. arXiv: 1308.4988.

Shen, Y. (2016). "Rest-Frame Optical Properties of Luminous $1.5 < z < 3.5$ Quasars: The Hβ-[O III] Region." In: *ApJ* in press. DOI: 10.1088/0004-6256/141/5/167. arXiv: 1512.00005.

Shen, Y. and L. C. Ho (2014). "The diversity of quasars unified by accretion and orientation." In: *Nature* 513, pp. 210–213.

Shen, Y. et al. (2011). "A Catalog of Quasar Properties from Sloan Digital Sky Survey Data Release 7." In: *ApJS* 194, p. 45.

Stockton, A. (1976). "The Structure and Spectrum of Nebulosity Associated with the QSO 4c 37.43." In: *ApJ* 205, p. L113. DOI: 10.1086/182102.

Sulentic, J. W., G. M. Stirpe, P. Marziani, R. Zamanov, M. Calvani, and V. Braito (2004). "VLT/ISAAC spectra of the Hβ region in

intermediate redshift quasars." In: *A&A* 423, pp. 121–132. DOI: 10.1051/0004-6361:20035912. eprint: astro-ph/0405279.

Veilleux, S. et al. (2013). "Fast Molecular Outflows in Luminous Galaxy Mergers: Evidence for Quasar Feedback from Herschel." In: *ApJ* 776, 27, p. 27. DOI: 10.1088/0004-637X/776/1/27. arXiv: 1308.3139.

Veron, M. P. (1981). "On the width and profile of nuclear emission lines in galaxies." In: *A&A* 100, pp. 12–19.

Vrtilek, J. M. (1985). "Seyfert galaxy narrow-line regions. II - Kinematic models." In: *ApJ* 294, pp. 121–133. DOI: 10.1086/163280.

Weedman, D. W. (1970). "High-Velocity Gas Motions in Galactic Nuclei." In: *ApJ* 159, p. 405. DOI: 10.1086/150318.

Whittle, M. (1985). "The narrow line region of active galaxies. I - Nuclear forbidden line profiles. II - Relations between forbidden line profile shape and other properties." In: *MNRAS* 213, pp. 1–31. DOI: 10.1093/mnras/213.1.1.

Yuan, S., M. A. Strauss, and N. L. Zakamska (2016). "Spectroscopic identification of type 2 quasars at $z < 1$ in SDSS-III/BOSS." In: *MNRAS* 462, pp. 1603–1615. DOI: 10.1093/mnras/stw1747. arXiv: 1606.04976.

Zakamska, N. L. and J. E. Greene (2014). "Quasar feedback and the origin of radio emission in radio-quiet quasars." In: *MNRAS* 442, pp. 784–804. DOI: 10.1093/mnras/stu842. arXiv: 1402.6736.

Zakamska, N. L., F. Hamann, I. Pâris, W. N. Brandt, J. E. Greene, M. A. Strauss, C. Villforth, D. Wylezalek, R. M. Alexandroff, and N. P. Ross (2016). "Discovery of extreme [O III] λ5007 Å outflows in high-redshift red quasars." In: *MNRAS* 459, pp. 3144–3160. DOI: 10.1093/mnras/stw718. arXiv: 1512.02642.

Zamanov, R., P. Marziani, J. W. Sulentic, M. Calvani, D. Dultzin-Hacyan, and R. Bachev (2002). "Kinematic Linkage between the Broad- and Narrow-Line-emitting Gas in Active Galactic Nuclei." In: *ApJ* 576, pp. L9–L13. DOI: 10.1086/342783. eprint: astro-ph/0207387.

Zhang, K., X.-B. Dong, T.-G. Wang, and C. M. Gaskell (2011). "The Blueshifting and Baldwin Effects for the [O III] λ5007 Emission Line in Type 1 Active Galactic Nuclei." In: *ApJ* 737, 71, p. 71. DOI: 10.1088/0004-637X/737/2/71. arXiv: 1105.1094 [astro-ph.CO].